IOPscience iopscience.iop.org

Home Search Collections Journals About Contact us My IOPscience

ESR study of spin–lattice correlated clusters in single crystalline $Nd_{0.7}Sr_{0.3}MnO_3$

This article has been downloaded from IOPscience. Please scroll down to see the full text article.

2007 J. Phys.: Condens. Matter 19 036207

(http://iopscience.iop.org/0953-8984/19/3/036207)

View the table of contents for this issue, or go to the journal homepage for more

Download details:
IP Address: 129.252.86.83
The article was downloaded on 28/05/2010 at 15:22

Please note that terms and conditions apply.

INSTITUTE OF PHYSICS PUBLISHING JOURNAL OF PHYSICS: CONDENSED MATTER

J. Phys.: Condens. Matter **19** (2007) 036207 (16pp) doi:10.1088/0953-8984/19/3/036207

ESR study of spin–lattice correlated clusters in single crystalline $Nd_{0.7}Sr_{0.3}MnO_3$

S Angappane[1,4], M Pattabiraman[1], G Rangarajan[1], K Sethupathi[1], Babu Varghese[2] and V S Sastry[3]

[1] Department of Physics, Indian Institute of Technology Madras, Chennai-600 036, India
[2] Sophisticated Analytical Instrumentation Facility, Indian Institute of Technology Madras, Chennai-600 036, India
[3] Materials Science Division, Indira Gandhi Centre for Atomic Research, Kalpakkam-603 102, India

E-mail: agpan@yahoo.com

Received 13 October 2006, in final form 2 December 2006
Published 5 January 2007
Online at stacks.iop.org/JPhysCM/19/036207

Abstract

We report electron spin resonance measurements in single crystalline $Nd_{0.7}Sr_{0.3}MnO_3$ that provide evidence for the existence of spin–lattice correlated clusters above and below T_C (=205 K). The linewidth of the paramagnetic spectrum indicates the presence of strong electron–phonon interaction rather than the spin only interaction seen in other manganites. The gradual increase observed in the g value above T_C is attributed to the presence of orbital correlations. The observation of ferromagnetic resonance (FMR) spectra only below 185 K ($T_C = 205$ K) and noisy features in the FMR spectra above 140 K are ascribed to the strong competition between localization due to lattice distortions and delocalization of charge carriers. The magnetocrystalline anisotropy of the sample splits the FMR line into two below 185 K. An additional splitting observed in the FMR line is attributed to the existence of spin–lattice correlated (insulating) clusters within the ferromagnetic (metallic) phase. The influence of these clusters on the spin dynamics above and below T_C is discussed.

1. Introduction

Perovskite manganites of the type $R_{1-x}A_xMnO_3$ (where R is the rare-earth ion, such as, La, Nd, Pr, etc and A is the divalent alkaline earth ion, such as, Ca, Sr, Ba, Pb, etc) exhibit colossal magnetoresistance upon application of magnetic fields of a few teslas [1, 2]. The

[4] Author to whom any correspondence should be addressed. Present address: Department of Physics, Sungkyunkwan University, Suwon 440-746, Korea.

 © 2007 IOP Publishing Ltd Printed in the UK

double exchange (DEX) interaction accounts for the ferromagnetic (FM) ground state of the manganites. However, several experimental results suggest that more complex ideas are needed to explain the main properties of these manganese oxides. For instance, above T_C and for a wide range of carrier densities, several manganites exhibit insulating behaviour of unclear origin that contributes to large magnetoresistance (MR). The phase diagram of these materials has a complex structure, not predicted by DEX, that includes insulating antiferromagnetic (AFM) and charge ordered (CO)/orbital ordered (OO) phases [3]. To understand the strong MR effects and the overall phase diagram of manganites, the DEX framework has been supplemented with more refined ideas. It has been shown that other interactions, such as electron–phonon interaction, inter-site exchange interaction between the e_g orbitals (orbital ordering tendency), intra-site and inter-site Coulomb repulsion interactions among the e_g electrons, AFM superexchange interaction between the t_{2g} local spins etc, compete with the ferromagnetic double exchange interaction and result in electronic phase separation [4]. Theoretical studies have shown that this competition is prominent close to alkaline earth concentrations of $x = 0$ (orbital ordered A-type AFM insulator) and 0.5 (charge/orbital ordered CE-type AFM insulator).

The development of theoretical ideas on phase separation has been motivated/aided by many experimental results that suggest the existence of magnetic inhomogeneities in manganese oxides either in macroscopic form or, more often, through the presence of nanoclusters of one phase embedded into another [5–7]. While it is not surprising to find such clusters close to the FM–AFM phase boundaries, recent results including our NMR and Raman scattering studies show that they are present well within the FM/AFM regions in manganites such as $Nd_{1-x}Sr_xMnO_3$.

For instance, $Nd_{0.7}Sr_{0.3}MnO_3$ (NSMO(0.3)) has an orthorhombic structure and undergoes a transition from a paramagnetic insulating state to a ferromagnetic metallic state at 205 K. NSMO(0.3) films exhibit a huge negative magnetoresistance ratio, $\frac{-\Delta R}{R(H)} \sim 10^6\%$, at 60 K in a magnetic field of 8 T—the largest colossal magnetoresistance effect ever reported [8]. ^{55}Mn NMR studies on NSMO(0.3) point to a coexistence of ferromagnetic metallic (FMM) and ferromagnetic insulating (FMI) regions below T_C [9]. Local lattice distortions arising from the Jahn–Teller interaction have been observed well below T_C from Raman scattering measurements in NSMO(0.3) [10]. Synchrotron x-ray scattering studies by Kiryukhin *et al* [11] reveal the presence of charge/orbitally ordered (COO) nanoclusters. Thus it is important to understand how the presence of these nanoclusters affects the temperature dependence of spin dynamics in NSMO(0.3).

We have performed X-band ESR measurements on an $Nd_{0.7}Sr_{0.3}MnO_3$ single crystal in order to address this issue. We also report the correlation among the diverse microscopic probes in order to understand more about the robust competition between carrier localizing and delocalizing mechanisms. Such a study is necessary for the theoretical formulation of phase separation in the ferromagnetic metallic state.

2. Experimental details

The NSMO(0.3) single crystal used in this study was grown by the floating zone method using a double ellipsoidal infrared image furnace and was made available to us by G Balakrishnan of the University of Warwick, UK. The crystal was characterized by x-ray diffraction, dc electrical resistivity and magnetization measurements.

Single crystal XRD data were collected using an Enraf-Nonius CAD-4 diffractometer [12]. The unit cell parameters are $a = 7.712(3)$ Å, $b = 7.723(5)$ Å, $c = 7.727(7)$ Å and the crystal system is orthorhombic. The structure solution was carried out using the computer

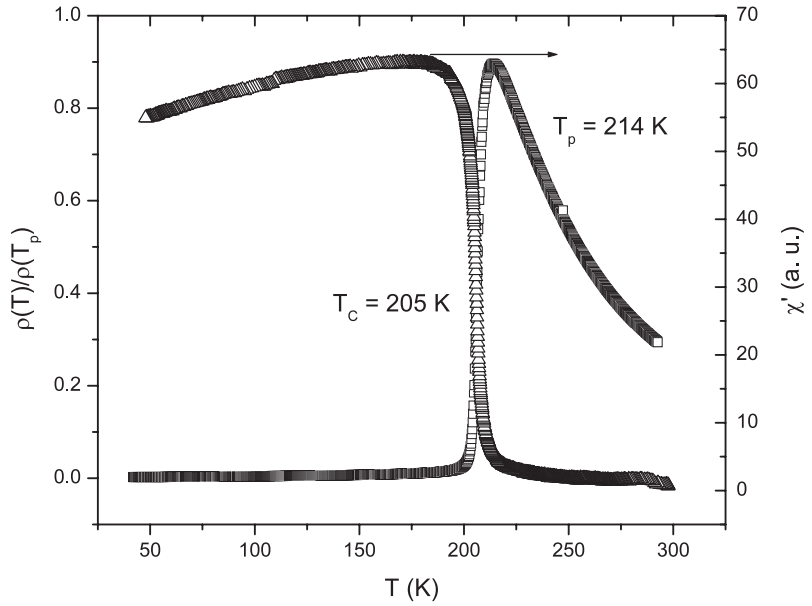

Figure 1. AC susceptibility and normalized resistivity versus temperature for NSMO(0.3) single crystal.

program SIR92 and the structure was refined using SHELXL-97 [13, 14]. Even though the cell parameters b and c are equal within the limits of standard deviation, none of the tetragonal space groups gave the refined structure. Then the structure solution and refinement were attempted with an orthorhombic space group *Pmmm* (which is the space group with the next highest symmetry) and it gave a sufficiently refined solution. The refinement of the structure was carried out with the sum of the occupancies of Nd and Sr in the unit cell constrained to 8 with Nd to 5.5 (∼70%) and Sr to 2.5 (∼30%). The refinement converged to a final R-factor of 6.5% and the occupancies of Nd and Sr ions are in the ratio of 69:31.

The temperature dependence of resistivity and ac magnetic susceptibility of the crystal (figure 1) shows the prototype paramagnetic–ferromagnetic ($T_C = 205$ K, derived from the temperature derivative of susceptibility) and insulator–metal transition (peak temperature, $T_p = 214$ K).

The crystal was ground into a spherical shape for the ESR measurements in order to eliminate demagnetization effects. The spherical shape was achieved by taking an approximately spherical sample (∼1 mm diameter) and grinding it in a ball mill for several days with micrometre sized alumina powder. The back-scattering Laue x-ray photograph method was employed to identify the crystallographic axes of the spherical crystal. The Laue photographs were taken along all three crystallographic axes. From the knowledge of parameters a, b and c the pattern which deviated more from the other two was taken as corresponding to the a-axis and among the other two axes, the one with the more symmetric Laue pattern was taken as the c-axis.

The ESR measurements were performed in the temperature range of 380–100 K by mounting the crystal on a copper sample rod attached to a goniometer. The c-axis was kept parallel to the magnetic field and for the angular dependence the crystal was rotated with respect to a-axis. 2,2-diphenyl(picryl hydrazyl) (DPPH) was used as the g marker.

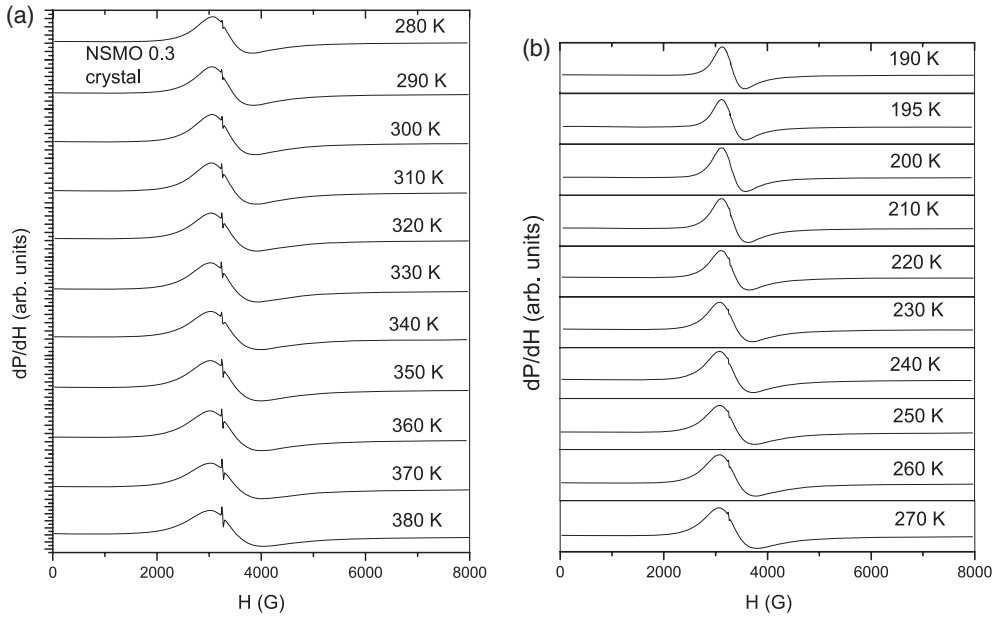

Figure 2. (a) ESR spectra of NSMO(0.3) crystal in the paramagnetic state between 380 and 280 K. (b) ESR spectra of NSMO(0.3) crystal in the paramagnetic state between 270 and 190 K.

3. Results

ESR spectra in the paramagnetic and ferromagnetic states are shown in figures 2(a), (b) and 3, respectively. A single asymmetric line was observed in the paramagnetic state. Although the T_C obtained from susceptibility measurement is 205 K, the spectrum splits into prominent low field and high field ferromagnetic resonance (FMR) lines only when the temperature was reduced to 185 K. The lines are well separated. A shoulder develops on the low field side of the low field line, grows in intensity with decreasing temperature and merges with the prominent low field line below 140 K. The high field line is broad and has structure. The spectra become less noisy below 130 K compared to the spectra above 140 K. The asymmetric ESR spectra could be fitted to asymmetric Lorentzian line shapes of the form [15],

$$\frac{\mathrm{d}P}{\mathrm{d}H} = \frac{\mathrm{d}}{\mathrm{d}H}\left[\frac{\Delta H + \alpha(H - H_0)}{(H - H_0)^2 + \Delta H^2}\right]. \tag{1}$$

This equation includes both absorption and dispersion, where α denotes the dispersion-to-absorption ratio. This has been derived from the general expression of Dyson [16] for the case of thick metallic samples with broad natural linewidth.

The paramagnetic spectra of the NSMO(0.3) crystal could be fitted to a single asymmetric Lorentzian line while four asymmetric Lorentzians were need to fit to the ferromagnetic spectra below 185 K. Though the high field (FMR) line 'appears' as a single line, it could not be fitted to a single asymmetric Lorentzian term and two asymmetric Lorentzian terms were needed. Figure 4 shows the typical fit to the ESR spectra along with the resolved lines. The temperature evolution of the spectra in the various temperature regions is discussed below.

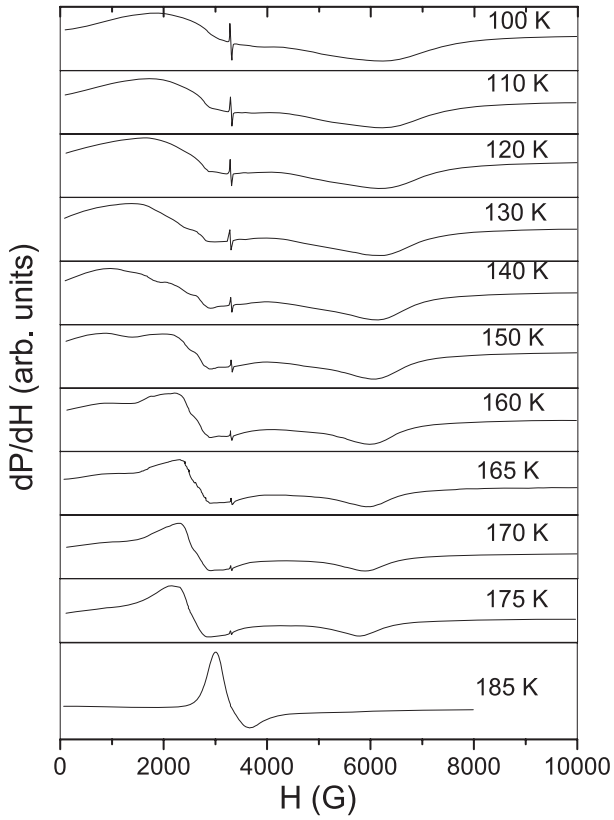

Figure 3. ESR spectra of NSMO(0.3) crystal in the ferromagnetic state below 185 K.

3.1. Paramagnetic state ($T > T_C$)

The skin depth is responsible for the observed asymmetric line shapes in the paramagnetic state of single crystalline NSMO(0.3). It was calculated using the formula $\delta = \sqrt{2\rho/\mu\omega}$ ($\rho_{dc} = 3 \times 10^{-5}$ Ω m at 300 K) and was found to be 0.02 mm, much less than the sample size of 1 mm diameter. The resonance field, linewidth and intensity were obtained by fitting the ESR spectra to the asymmetric Lorentzian equation (equation (1)). The g value was calculated with respect to the DPPH line. It increases from 2.00 to 2.03 as the temperature decreases from 380 to 195 K (figure 5). Such behaviour is unusual in the paramagnetic state and it may arise from additional spin correlations.

Though there are reports on the presence of spin clusters in the paramagnetic state of many ferromagnetic metallic manganites [17], none have reported an increase in g value in the paramagnetic state. In an attempt to seek an explanation for the observed behaviour, we note that orbital degrees of freedom can also bring about an increase in g in the paramagnetic state. For example, a prominent increase in the g value of $Nd_{0.5}Ca_{0.5}MnO_3$ is observed in its charge/orbital ordered state ($T_{CO} = 240$ K), well above the Néel temperature ($T_N = 140$ K) [18]. Orbital degrees of freedom in $LiCuVO_4$ manifest as an increase in g value in the paramagnetic state [19].

Considering these results, we suggest that orbital degrees of freedom may influence the spin correlations in the paramagnetic state of NSMO(0.3). The present results are significant

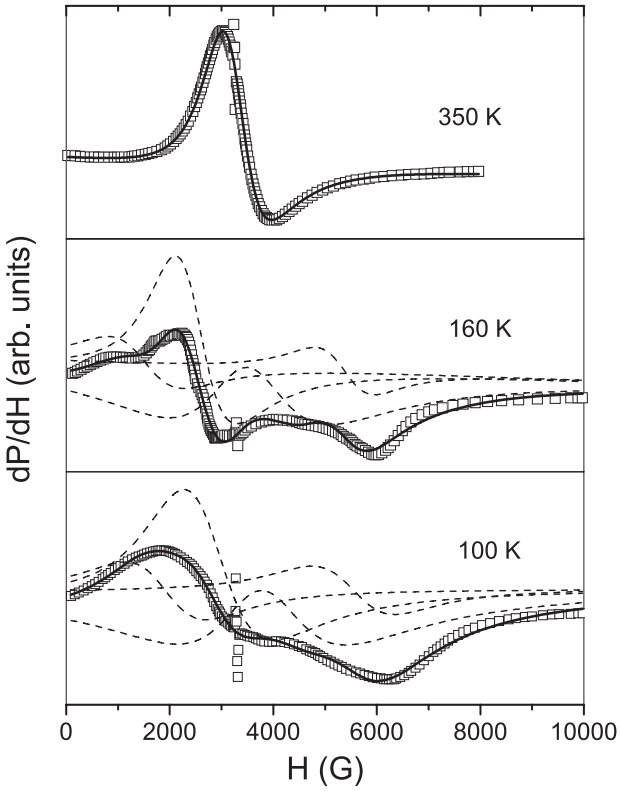

Figure 4. Representative spectra with fitted and resolved curves at various temperatures. The solid lines are the fitted curves and the dashed lines are resolved curves.

because, unlike the case of NSMO(0.5) for which we reported a similar result [20], NSMO(0.3) is expected to be an orbital disordered ferromagnetic metal down to 0 K.

3.1.1. ESR linewidth in paramagnetic state. The linewidth of the ESR spectrum in the paramagnetic state (figure 6) increases linearly above T_C. In order to understand this behaviour we note that the literature on ESR studies in manganites records three interpretations of the temperature dependence of the paramagnetic ESR linewidth as follows. (a) A spin-only relaxation mechanism proposed by Causa *et al* [17] resulting in a 'universal' quasilinear temperature dependence of the linewidth. The quasilinear linewidth arises from the presence of paramagnetic spin clusters and is dominated by the variations of $\chi(T)$,

$$\Delta H_{pp}(T) = \Delta H_{pp}(\infty)\left(\frac{C}{T\chi}\right) \tag{2}$$

where C/T is the single-ion (Curie) susceptibility, χ is the measured paramagnetic susceptibility of magnetically coupled clusters and $\Delta H_{pp}(\infty)$ is the linewidth expected at temperatures high enough for the dc susceptibility to follow a Curie–Weiss law. (b) An exchange mechanism with bottlenecked spin relaxation between Mn^{3+} and Mn^{4+} ions proposed by [21]. (c) A spin–phonon coupling proposed by Seehra *et al* [22].

A clear deviation from the quasilinear temperature dependence proposed by Causa *et al* (model (a)) was observed (inset, figure 6). Model (b) is not valid here, as there is no activated

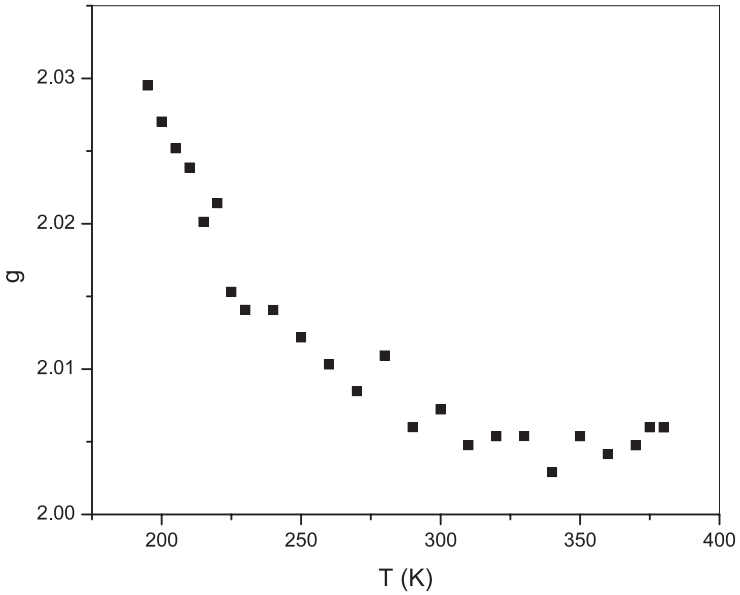

Figure 5. Temperature dependence of g for NSMO(0.3) crystal.

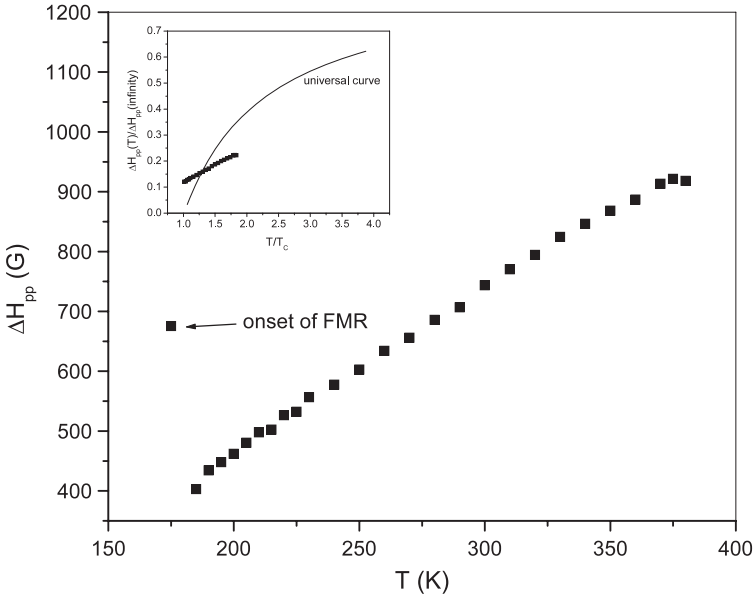

Figure 6. ΔH_{pp} versus temperature for NSMO(0.3) single crystal. The inset shows $\Delta H_{pp}(T)/\Delta H_{pp}(\infty)$ versus temperature for NSMO(0.3) and universal dependence of $\Delta H_{pp}(T)/\Delta H_{pp}(\infty)$ for manganites.

temperature dependence which is associated with the bottleneck mechanism [23]. Model (c) is found to agree with the observed linear variation of $\Delta H_{pp}(T)$.

Seehra *et al* [22] (model c) explained a linear dependence of linewidth in manganites using a mechanism including critical and non-critical contributions. The non-critical contribution

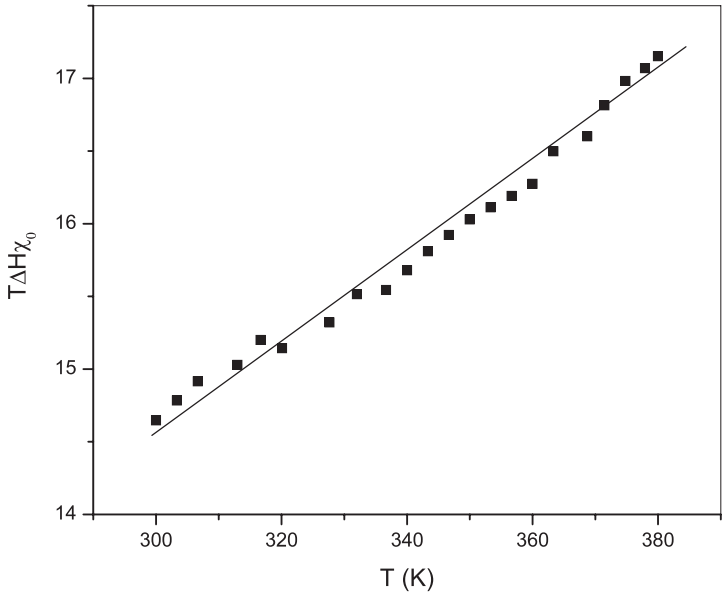

Figure 7. Temperature dependence of the product $T\Delta H\chi_0$ for NSMO(0.3) crystal. The solid line is a guide to the eye.

arises from the spin–spin interactions for $T \gg T_C$ whereas the critical contribution is due to the spin–phonon interaction. The resulting expression has the form

$$\Delta H = \frac{\hbar[c + f(\varepsilon)]}{g\mu_B T\chi_0} \tag{3}$$

where μ_B is the Bohr magneton, $\hbar$ is Planck's constant, $f(\varepsilon)$ is the critical contribution to ΔH which is significant only for $\varepsilon = (T - T_C)/T_C \geqslant 0.1$ and c is the non-critical contribution from spin–spin interactions for $T \gg T_C$. If there is no contribution to the linewidth from sources other than spin–spin interactions, c would approach a temperature independent value for $T \gg T_C$. In this case, the product $\Delta H T\chi_0$ would approach a temperature independent constant value for $T \gg T_C$. To investigate this, a plot of the product of $\Delta H T\chi_0$ versus T is shown in figure 7 and it is found to increase with an increase of temperature. Then, following the discussion of Seehra *et al* [22] it is inferred that the observed temperature dependence of linewidth is due to the spin–phonon coupling in the paramagnetic state of the NSMO(0.3) crystal.

3.1.2. Intensity of the paramagnetic ESR spectrum. The double integrated intensity of the ESR spectrum was calculated using the formula:

$$I \propto \Delta H_{pp}^2 Y' \tag{4}$$

where $2Y'$ is the peak-to-peak derivative amplitude. The intensity is found to decrease exponentially as the temperature increases (figure 8). This is characteristic of the presence of spin clusters. The intensity can be described using the expression $I = I_0 e^{-\Delta E/k_B T}$, where ΔE is the energy required to dissociate the spin clusters [24]. From the plot of ln(intensity) versus temperature (inset figure 8) ΔE is found as 0.06 eV.

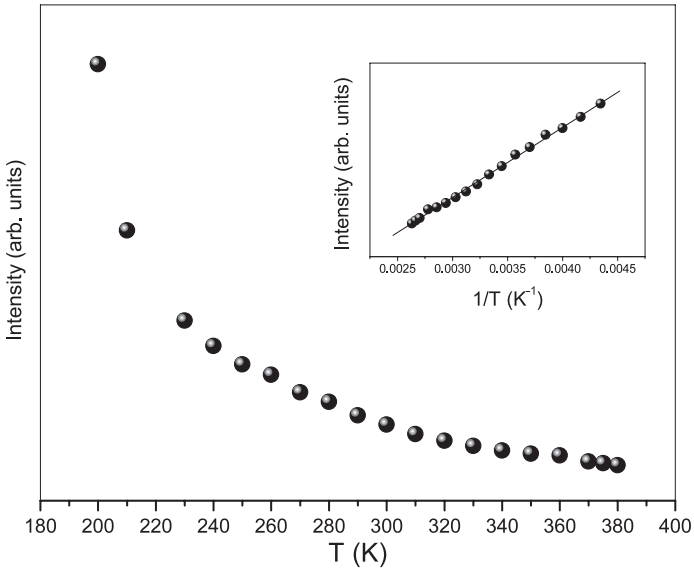

Figure 8. Plot of intensity of ESR spectra versus temperature for NSMO(0.3) single crystal. The exponential decrease of the PM intensity also points to the existence of spin clusters. The inset shows the straight line fit to ln(intensity) versus temperature (Arrhenius equation). The activation energy ΔE is found to be 0.06 eV.

3.2. Ferromagnetic state ($T < 185$ K)

The best fit to the spectra below 185 K was obtained with an equation consisting of four asymmetric Lorentzians (equation (1)). The quality of the fit was found to improve below 130 K. Figure 9 shows the ESR resonance fields derived from the fits. The resonance fields of the lines named $H1$, $H2$, $L1$ and $L2$ are nearly constant.

Multiple ESR lines below 185 K could arise from two mechanisms: (1) coexisting magnetic phases and (2) magnetocrystalline anisotropy of the sample, when the field is not applied along the easy direction of magnetization. We have shown that rotating the sample with respect to the applied magnetic field is good way of differentiating between the two mechanisms [20]. If the line splitting arises from coexisting phases, there should not be significant angular dependence of the ESR spectra, whereas the magnetocrystalline anisotropy of the sample induces a periodic variation of the high field resonance line depending on the direction of orientation of the crystallographic axes with respect to the applied magnetic field.

In order to investigate the origin of the resonance lines below T_C, angle dependent ESR measurements of the NSMO(0.3) crystal were made at 100 K. The spherical shape of the sample nullifies the demagnetizing effects. Though a clear angular variation is observed at 100 K (figure 10), the positions of the high field resonance line do not exhibit a systematic angular variation (figure 11). To understand the origin of the angular dependence we fit the spectrum to two asymmetric Lorentzians, treating the pair of high field lines ($H1$ and $H2$) and low field lines ($L1$ and $L2$) as two broad envelopes H' and L'. A typical two-line fit to the 100 K data corresponding to 0° is shown in figure 12.

The resonance fields L' and H' exhibit a periodic angular variation as shown in figure 13. It is an approximate $\cos 4\varphi$ variation with maxima at 0°, 90° and 180° and minima at 45° and 135° which resembles the dependence of the resonance field on the angle φ between applied field (H) and the [100] axis in the (010) plane for a cubic crystal. Such an approximate $\cos 4\varphi$

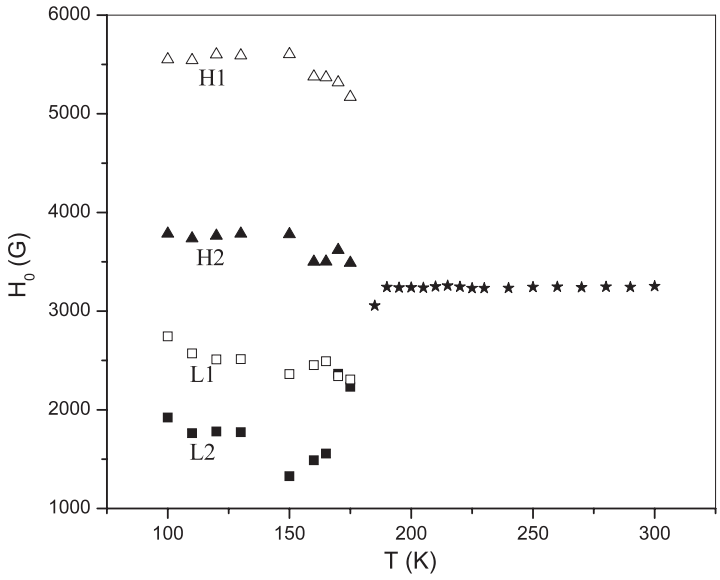

Figure 9. Resonance field versus temperature of NSMO(0.3) single crystal.

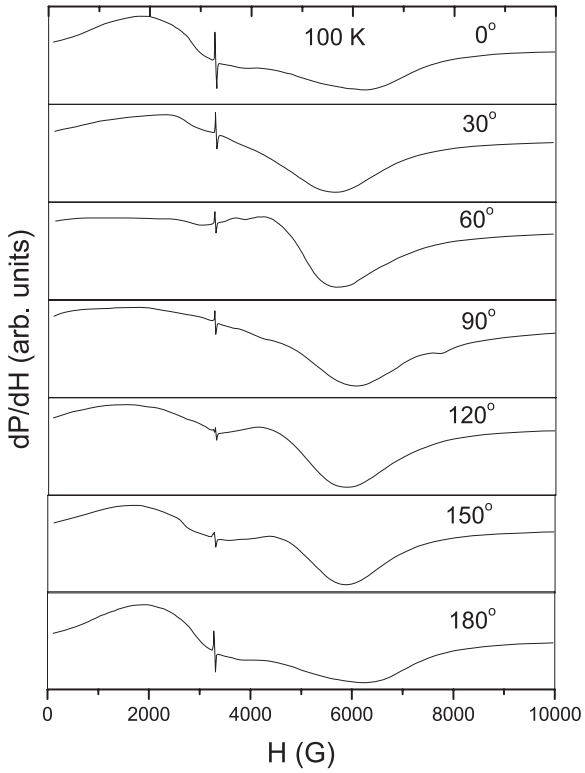

Figure 10. Angular variation of ESR spectra of NSMO(0.3) crystal at 100 K.

angular dependence of the resonance field may occur if the unit cell of NSMO(0.3) may be thought of as a 'pseudo cube' (with local *Pmmm* symmetry). Thus figure 13 suggests that the

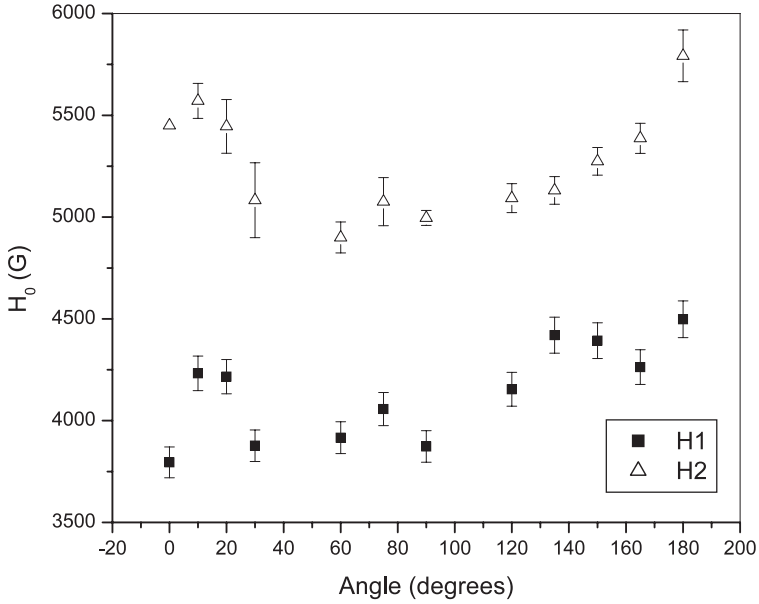

Figure 11. Angular dependence of the high field line of the resonance fields of NSMO(0.3) crystal at 100 K. The high field line was resolved into two asymmetrical Lorentzians (equation (1)).

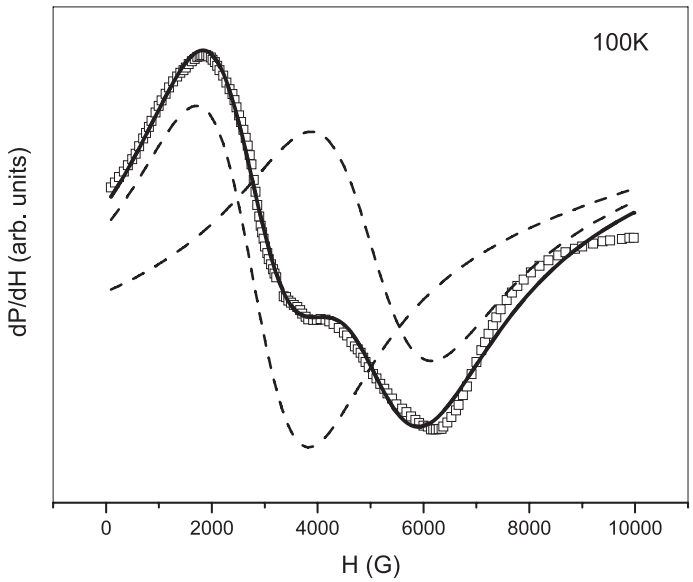

Figure 12. Typical two-line resolution of the 100 K ESR spectrum of NSMO(0.3) crystal. The solid line is the fit and the dotted lines are the resolved lines.

broad low-field and high-field envelopes (L' and H') arise as a result of magnetocrystalline anisotropy. Although the FMR envelopes (L' and H') arise as a result of magnetocrystalline anisotropy, they can be further resolved into two pairs of lines ($L1$, $L2$ and $H1$, $H2$). The origin of these FMR lines, the temperature dependence of the FMR spectrum and its angular variation are discussed further in the next section.

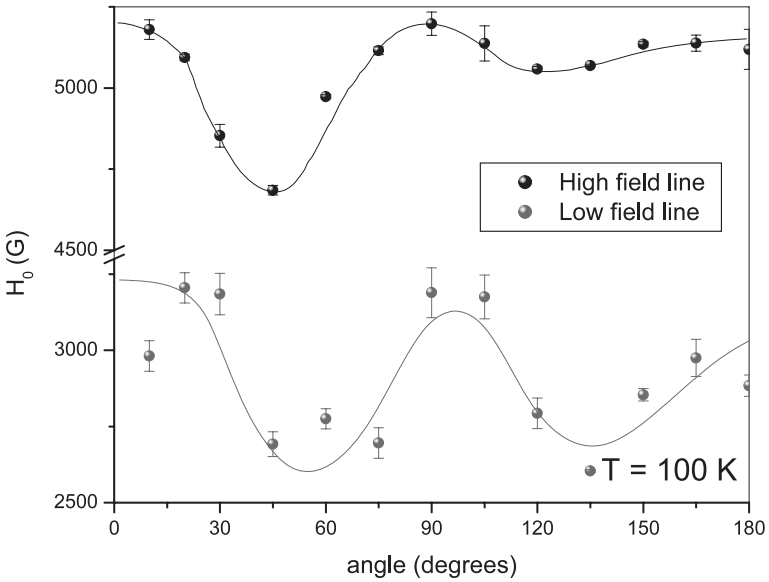

Figure 13. Angular dependence of the resonance field of high field and low field envelopes of NSMO(0.3) crystal at 100 K. The solid lines are guides to the eye.

4. Discussion

In order to obtain a clear insight into the temperature evolution of spin dynamics in NSMO(0.3) and to understand the above results better we compare the temperature evolution of the ESR, NMR, Raman and synchrotron data of $Nd_{0.7}Sr_{0.3}MnO_3$ below T_C.

The temperature dependence of the linewidth of the phonon mode around 66 cm^{-1} (M_1: related to the vibration of Nd cations in the XX Raman spectrum exhibits a sharp decrease around 150 K in single crystalline NSMO(0.3) (figure 14(a))) [10]. This is likely to arise from the decrease in the collision-dominated contribution due to spin fluctuations that occur in the Raman spectrum below 100 cm^{-1} and is a signature of suppression of spin disorder and enhanced carrier mobility. Zero-field ^{55}Mn spin-echo NMR measurements on polycrystalline NSMO(0.3) also lend support to this view [9]. The NMR spectrum is multi-peaked like the FMR spectrum. Therefore, the spectral centre of gravity is used to understand its temperature evolution.

The temperature dependence of the centre of gravity of the NMR spectrum, defined as $\frac{\sum_i a_i \omega_i}{\sum_i a_i}$ where a_i corresponds to the spin-echo amplitude at frequency ω_i, exhibits a kink that coincides with the decrease in linewidth of M_1 (figure 14(b)). The centre of gravity of the NMR spectrum is expected to exhibit critical behaviour and is proportional to the evolution of spin ordering in the lattice. The kink in the centre of gravity corresponds to a decrease in intensity of a spin-echo signal (∼330 MHz) corresponding to ferromagnetic insulating regions (figure 14(b) open circles) and the appearance of a signal around 350–360 MHz corresponding to the hopping of e_g electrons between Mn^{3+} and Mn^{4+}. Both observations point to an abrupt increase in spin order as well as electron mobility via the double exchange interaction. The low frequency spin-echo peak increases linearly with decrease in temperature, again suggestive of gradual spin order below T_C. Reference [9] may be consulted for further details.

The centre of gravity of the ESR spectrum was computed in order to compare the ESR spectra with the NMR and Raman data. The centre of gravity of the spectrum defined as $\frac{\sum_i A_i H_i}{\sum_i A_i}$,

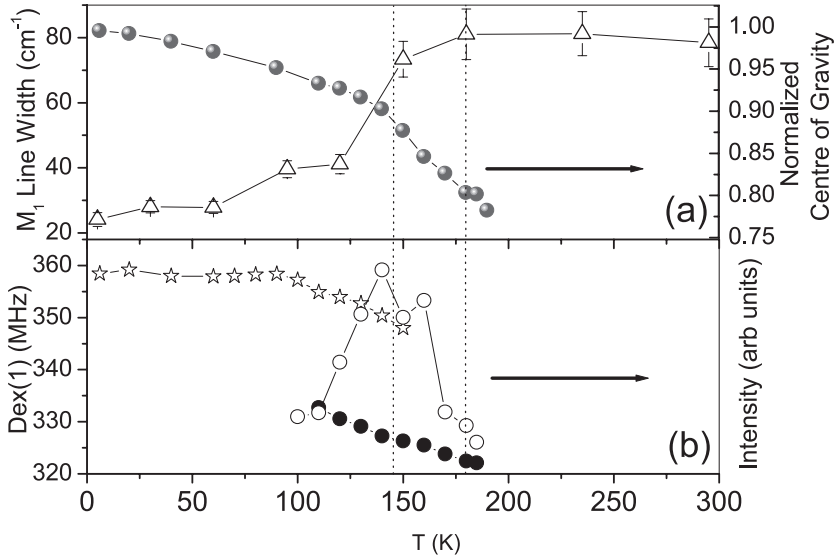

Figure 14. (a) Plot of the linewidth of the phonon mode around 66 cm^{-1} (M_1: related to the vibration of Nd cations) in the XX Raman spectrum and centre of gravity of the ^{55}Mn spin-echo NMR spectrum versus temperature. (b) Temperature dependence of DEX and FMI spin-echo peak frequencies and intensity of the FMI peak.

where A_i corresponds to the absorption amplitude observed at a field H_i, was calculated after integrating the recorded first-derivative spectrum. From figure 15, where the ESR spectra at representative temperatures are also plotted, it is seen that between T_C and 140 K the centre of gravity has no systematic temperature dependence. Below 140 K, the centre of gravity increases smoothly. This observation again indicates an abrupt increase in spin order below 140 K.

This striking correspondence of the temperature evolution of spin dynamics in NSMO(0.3) as observed from different microscopic probes combined with the observation of spin clusters that are strongly coupled to lattice degrees of freedom, possibly with orbital correlations in the paramagnetic state, suggests that the spin clusters are strongly correlated with each other and significantly influence the spin dynamics in NSMO(0.3).

Such clusters have been recently observed by x-ray synchrotron measurements [11]. Well-defined satellite peaks have been observed in the region surrounding Bragg peaks where butterfly shaped diffuse scattering from independent polarons is present in momentum space. In some cases, these peaks are located at the position corresponding to the CE state. Thus, the satellite peaks are assigned to small charge/orbital ordered clusters with a size of the order of nanometres which coexist with independent polarons in the paramagnetic state. Using ESR data, we show how the presence of these clusters influences the ferromagnetic state. The temperature dependence of the intensity of the peak due to structural correlations observed by Kiryukhin *et al* [11] in NSMO(0.3) is shown in figure 16. The peak intensity reflects the content of the correlated regions. The ESR spectra at specific temperatures are shown as insets. The onset of the FMR signal does not correspond to T_C as observed from magnetization measurements (=205 K) or to the metal–insulator transition temperature ($T_p = 214$ K) but to the abrupt decrease in the intensity of the structurally correlated peak below 185 K. Thus, the onset of the ferromagnetic state can be thought of as arising from a competition between the double exchange mechanism and the strong coupling between the lattice, spin and orbital degrees of freedom. The persistence of the structurally correlated peak below T_C shows that

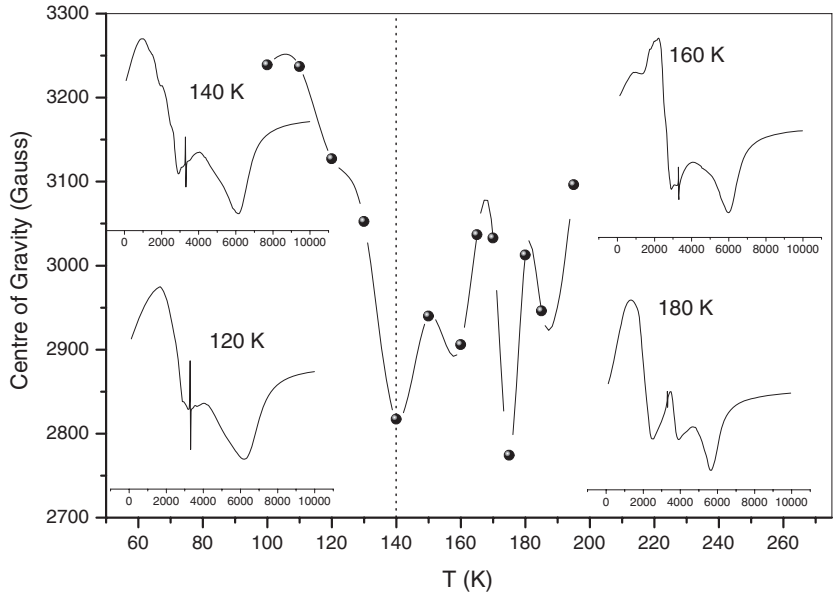

Figure 15. The centre of gravity of the ESR spectrum versus temperature. The inset shows the ESR spectrum at representative temperatures.

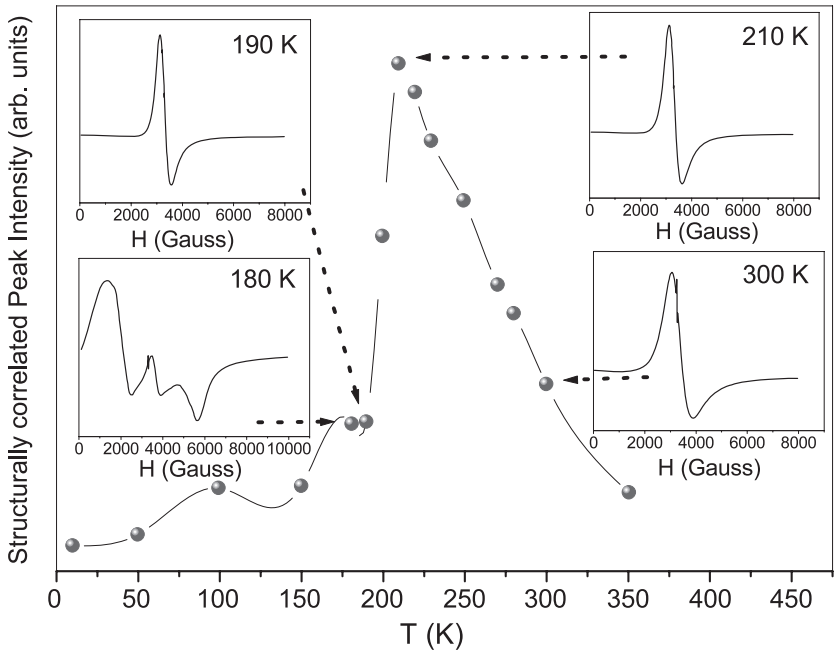

Figure 16. Temperature dependence of the structurally correlated synchrotron peak observed for $Nd_{0.7}Sr_{0.3}MnO_3$ [11]. The insets show the observed ESR spectrum at representative temperatures.

this competition persists in the ferromagnetic state. The correlations observed among the ESR, NMR and Raman measurements around 140–150 K suggest that there is a further abrupt decrease in the concentration of the correlated clusters resulting in enhanced spin order.

The synchrotron data shows that the correlated regions persist well above T_C and are observed up to the highest measurement temperature (350 K). This supports the activation energy of 60 meV (696 K) obtained from the intensity data (figure 8) and points to the robustness of the clusters.

The angular dependence of the high field and low field envelopes (figure 13) shows the presence of magnetic anisotropy in $Nd_{0.7}Sr_{0.3}MnO_3$. What is its origin? We have shown how the presence of magnetic anisotropy affects the ESR spectrum in $Nd_{0.5}Sr_{0.5}MnO_3$ [20]. Both compounds exhibit a gradual increase in the g value in the paramagnetic state possibly due to orbital correlations. Nanoscale correlated lattice distortions have been observed in both compounds by synchrotron measurements [11]. Hard x-ray scattering studies on $Nd_{0.5}Sr_{0.5}MnO_3$ reveal the presence of anisotropic CE-type orbital correlations in the ferromagnetic metallic phase [25]. These results suggest the possibility that the structurally correlated spin clusters may render the ferromagnetic state anisotropic in $Nd_{0.7}Sr_{0.3}MnO_3$, resulting in low-field and high-field envelopes (L' and H'). Each anisotropy-split envelope is further split into two, resulting in four lines ($H1$, $H2$ and $L1$, $L2$). We interpret this splitting as arising from the phase coexistence of ferromagnetism and correlated clusters (in addition to the effect of anisotropy), resulting in multiple internal fields and an inhomogeneous ferromagnetic state. This conclusion is strongly supported by our NMR study [9]. There is similar evidence from ESR [26] and several other experiments in the manganite literature [5–7] that phase coexistence driven by the complex interplay among spin, lattice, charge and orbital degrees of freedom [4] results in magnetic inhomogeneity.

Thus it is clear that the correlated clusters significantly influence the spin dynamics in the paramagnetic and ferromagnetic state in $Nd_{0.7}Sr_{0.3}MnO_3$. Further work is required to understand the mechanism leading to the formation of correlated spin clusters.

5. Conclusions

The ESR study of single crystalline $Nd_{0.7}Sr_{0.3}MnO_3$ reveals the presence of spin–lattice correlated clusters above and below T_C. The linewidth of the paramagnetic spectrum indicates the presence of strong electron–phonon interaction rather than the spin only interaction seen in other manganites. The gradual increase in the g value above T_C is attributed to the presence of orbital correlations. Below T_C, the sample behaves like an anisotropic ferromagnetic solid in which the field due to the magnetocrystalline anisotropy splits the FMR spectra. A further splitting in the FMR line is attributed to the presence of clusters with charge and/or orbital correlations in the ferromagnetic conducting state. The observation of FMR spectra only below 185 K ($T_C = 205$ K) and noisy features in the FMR spectra above 140 K are attributed to the strong competition between localization due to lattice distortions and delocalization of charge carriers. We have studied this strong competition between the correlated clusters and the ferromagnetic phase by comparing the present ESR results with reported NMR, Raman and synchrotron data and showed how these clusters significantly influence the spin dynamics above and below T_C.

In summary, temperature dependent ESR study of the NSMO(0.3) single crystal shows the significance of the correlated clusters in the understanding of the paramagnetic insulating to ferromagnetic metallic transition and the coexisting phases in the ferromagnetic metallic state.

Acknowledgment

The authors thank N Sivaramakrishnan, Sophisticated Analytical Instrument Facilities, Indian Institute of Technology Madras for assistance in ESR measurements.

References

[1] von Helmholt R, Wecker J, Holzapfel B and Samwer K 1993 *Phys. Rev. Lett.* **71** 2331
[2] Jin S, McCormack M, Tiefel T H and Ramesh R 1994 *J. Appl. Phys.* **76** 6929
[3] Tokura Y 2000 *Colossal Magnetoresistive Oxides* ed Y Tokura (Singapore: Gordon and Breach)
[4] Dagotto E, Takashi H and Moreo A 2001 *Phys. Rep.* **344** 1
[5] Papavassiliou G, Fardis M, Belesi M, Panagiotopoulos I, Kallias G, Niarchos D, Dimitropoulos C and Dolinsek J 2000 *Phys. Rev. Lett.* **84** 761
[6] De Teresa J M, Ibarra M R, Algarabel P A, Ritter C, Marquina C, Blasco J, Garcia J, del Moral A and Arnold Z 1997 *Nature* **386** 256
[7] Uehara M, Mori S, Chen C H and Cheong S-W 1999 *Nature* **399** 560
[8] Xiong C, Li Q, Ju H L, Mao S N, Senapati L, Xi X X X, Green R L and Venkatesan T 1995 *Appl. Phys. Lett.* **66** 1427
[9] Pattabiraman M, Murugaraj P, Rangarajan G, Dimitropoulos C, Ansermet J-Ph, Papavassiliou G, Balakrishnan G, McK Paul D and Lees M R 2002 *Phys. Rev.* B **66** 224415
[10] Choi K-Y, Lemmens P, Güntherodt G, Pattabiraman M, Rangarajan G, Gnezdilov V P, Balakrishnan G, McK Paul D and Lees M R 2003 *J. Phys.: Condens. Matter* **15** 1
[11] Kiryukhin V, Koo T Y, Borissov A, Kim Y J, Nelson C S, Hill J P, Gibbs D and Cheong S-W 2002 *Phys. Rev.* B **65** 094421
[12] 1989 *Enraf-Nonius CAD-4 software, Version 5.0* Enraf-Nonius, Delft, The Netherlands
[13] Sheldrick G M 1997 *SHELXL97 and SHELXS97* University of Gottingen, Germany
[14] Spek A L 1999 *PLATON for Windows* Utretch University, The Netherlands
[15] Ivanshin V A, Deisenhofer J, Krug von Nidda H-A, Loidl A, Mukhin A A, Balbashov A M and Eremin M V 2000 *Phys. Rev.* B **61** 6213
[16] Dyson F J 1955 *Phys. Rev.* **98** 349
[17] Causa M T, Tovar M, Canerio A, Prado F, Ibanez G, Ramos C A, Butera A, Alascio B, Obradors X, Pinol S, Rivadulla F, Vasquez-Vazquez C, Lopez-Quintela M A, Rivas J, Tokura Y and Oseroff S B 1998 *Phys. Rev.* B **58** 3233
[18] Joshi J P, Gupta R, Sood A K, Bhat S V, Raju A R and Rao C N R 2002 *Phys. Rev.* B **65** 024410
[19] Krug von Nidda H-A, Svistov L E, Eremin M V, Eremina R M, Loidl A, Kataev V, Validov A, Prokofiev A and Assmus W 2002 *Phys. Rev.* B **65** 134445
[20] Angappane S, Pattabiraman M, Rangarajan G, Sethupathi K and Sastry V S 2004 *Phys. Rev.* B **69** 094437
[21] Shengelaya A, Zhao G-M, Keller H and Müller K A 1996 *Phys. Rev. Lett.* **77** 5296
[22] Seehra M S, Ibrahim M M, Suresh Babu V and Srinivasan G 1996 *J. Phys.: Condens. Matter* **8** 11283
[23] Shengelaya A, Zhao G-M, Keller H, Müller K A and Kochelaev B I 2000 *Phys. Rev.* B **61** 5888
[24] Angappane S, Rangarajan G and Sethupathi K 2003 *J. Appl. Phys.* **93** 8334
[25] Geck J, Bruns D, Hess C, Klingeler R, Reutler P, Zimmermann M V, Cheong S-W and Büchner B 2002 *Phys. Rev.* B **66** 184407
[26] Joh K W, Lee C H, Lee C E, Hur N H and Ri H-C 2003 *J. Phys.: Condens. Matter* **15** 4161